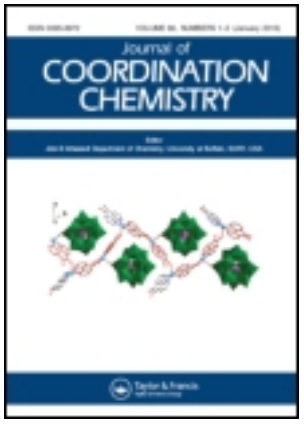

Journal of Coordination Chemistry
Publication details, including instructions for authors and subscription information:
http://www.tandfonline.com/loi/gcoo20

Copper coordination complexes of bis(4-(pyridin-2-yl)pyrimidin-2-ylthio)methane with in situ metal redox reactions

Hai-Bin Zhu [a b], Xin Lu [a], Wen-Na Yang [a] & Shu-Ying Zhang [a]

[a] Pharmaceutical Research Center, School of Chemistry and Chemical Engineering, Southeast University, Nanjing 211189, China

[b] Jiangsu Province Hi-Tech Key Laboratory for Bio-Medical Research, Nanjing 211189, China

Published online: 15 May 2012.

To cite this article: Hai-Bin Zhu, Xin Lu, Wen-Na Yang & Shu-Ying Zhang (2012) Copper coordination complexes of bis(4-(pyridin-2-yl)pyrimidin-2-ylthio)methane with in situ metal redox reactions, Journal of Coordination Chemistry, 65:12, 2087-2097, DOI: 10.1080/00958972.2012.687730

To link to this article: http://dx.doi.org/10.1080/00958972.2012.687730

Journal of Coordination Chemistry
Vol. 65, No. 12, 20 June 2012, 2087–2097

Taylor & Francis
Taylor & Francis Group

Copper coordination complexes of bis(4-(pyridin-2-yl)pyrimidin-2-ylthio)methane with *in situ* metal redox reactions

HAI-BIN ZHU*†‡, XIN LU†, WEN-NA YANG† and SHU-YING ZHANG†

†Pharmaceutical Research Center, School of Chemistry and Chemical Engineering, Southeast University, Nanjing 211189, China
‡Jiangsu Province Hi-Tech Key Laboratory for Bio-Medical Research, Nanjing 211189, China

(*Received 9 November 2011; in final form 12 March 2012*)

Five copper coordination complexes **1**–**5** with **2-bppm** (**2-bppm** = bis(4-(pyridin-2-yl)pyrimidin-2-ylthio)methane) have been prepared and structurally elucidated. Complexes **1** and **2** are both discrete dinuclear [2 + 2] macrocyclic structures, simultaneously formed in one-pot reaction with $Cu(NO_3)_2$ with *in situ* reduction of Cu^{2+}. Similarly, dinuclear [2 + 2] macrocyclic motifs are found with **3** and **4**, which are also obtained by one-pot reaction but with CuCl accompanied by *in situ* air oxidation of Cu^{+}. Compound **5** exhibits a 1-D chain structure with **2-bppm** and Cu_2I_2 connected one by one. Luminescence is measured for **2**, **4**, and **5**, all based on d^{10}-closed shell Cu(I).

Keywords: Copper; Dinuclear; Macrocycle; Redox

1. Introduction

Although crystal engineering has advanced [1–3], control over the self-assembly process still remains a great challenge. Judicious selection of metal ions and organic linkers enables prediction to some extent; however, the final result often deviates from the expected largely because of subtle factors such as temperature, concentration, and pH. Redox-active metal ions make this issue more intractable since structures of metal ions vary with valence state. Furthermore, flexible organic linkers pose more challenges over the control of assembly than rigid counterparts such as 4,4′-bipyridine [4], making possible self-adjusting spatial arrangement of the coordination donors in response to environment changes, which allows for better understanding of the assembly process [5, 6].

We have been engaged in studying coordination chemistry about heterocyclic disulfides [7, 8] together with their *in situ* metal/ligand reactions [9–11] in an effort to control these processes. In contrast with the semi-rigid disulfide ligands, we report

*Corresponding author. Email: zhuhaibin@seu.edu.cn

ISSN 0095-8972 print/ISSN 1029-0389 online
http://dx.doi.org/10.1080/00958972.2012.687730

herein coordination of the flexible **2-bppm**, namely bis(4-(pyridin-2-yl)pyrimidin-2-ylthio)methane, of which two rigid bipyridine-like compartments are joined *via* an –S–CH_2–S– linking unit. In our previous investigation, assembly of AgX salts ($X = NO_3^-$, BF_4^-) with **2-bppm** resulted in two isostructural dinuclear [2 + 2] macrocyclic coordination complexes, of which **2-bppm** exclusively uses nitrogen as the coordination donors [12]. One reason for –S–CH_2–S– spacer free of Ag coordination is that the potent *NN*-chelating mode of **2-bppm** competes against the weakly coordinating S of thioether [13, 14]. In this report, copper salts are selected for reaction with the flexible **2-bppm** giving interesting structural variations concurrent with copper redox phenomena.

2. Experimental

2.1. *Materials and measurements*

Analytical grade reagents were used as received. **2-bppm** was prepared according to our reported procedure [12]. Elemental analyses for C, H, and N were performed on a CHN-O-Rapid analyzer and an Elementar Vario MICRO analyzer. Infrared (IR) spectra were performed on a Bruker Vector 22 spectrophotometer with KBr pellets from 400 cm^{-1} to 4000 cm^{-1}. UV-Vis spectra were conducted on a Shimadzu UV-1700 UV-Vis Spectrometer. The luminescence spectra for solid samples were recorded at room temperature on an Aminco Bowman Series 2 spectrophotometer.

2.2. *Synthesis*

2.2.1. General procedure. A methanol solution (5 mL) of metal salts (0.1 mmol) was carefully layered above a CH_2Cl_2 solution (5 mL) of **2-bppm** (0.1 mmol). Crystals were afforded after 2 weeks. The crystals were collected and dried under vacuum. Single-crystals suitable for X-ray diffraction were selected.

Complexes **1** and **2**, obtained as a mixture, were separated manually according to their different colors (**1**: green crystals; **2**: red crystals). Complex **1**: Yield 42%. Anal. Calcd for $C_{38}H_{32}Cu_2N_{16}O_{14}S_4$: C, 38.29; H, 2.71; N, 18.80. Found: C, 38.21; H, 2.69; N, 18.55%. IR(KBr) ν_{max}/cm^{-1}: 3069m, 1567m, 1544m, 1484m, 1452m, 1414s, 1384s, 1339s, 1294m, 1192m, 1092s, 1031m, 827w, 797m, 762m, 720m. Complex **2**: Yield 7%. Anal. Calcd for $C_{38}H_{26}Cu_2N_{14}O_6S_4$: C, 44.31; H, 2.54; N, 19.04. Found: C, 44.35; H, 2.79; N, 19.35%. IR(KBr) ν_{max}/cm^{-1}: 3067m, 1565s, 1543m, 1417m, 1384s, 1340s, 1188m, 1111m, 795m, 760m, 719 ms.

Complexes **3** and **4** were readily separated since they formed in different regions (**3** in the upper layer and **4** in the lower layer). Complex **3**: Yield 31%. Anal. Calcd for $C_{40}H_{33}Cl_6Cu_3N_{13}OS_4$: C, 38.64; H, 2.68; N, 14.64. Found: C, 38.55; H, 2.73; N, 14.55%. IR(KBr) ν_{max}/cm^{-1}: 3070m, 1567s, 1542s, 1415s, 1340s, 1197s, 796m, 761s, 722m. Complex **4**: Yield 23%. Anal. Calcd for $C_{38}H_{28}Cl_2Cu_2N_{12}S_4$: C, 46.62; H, 2.88; N, 17.17. Found: C, 46.65; H, 2.79; N, 17.35%. IR(KBr) ν_{max}/cm^{-1}: 3060m, 1564s, 1542s, 1421s, 1346s, 1187m, 790m, 758s, 717m.

Complex **5** precipitated at the bottom of the reaction vessel and was collected by simple filtration. Complex **5**: Yield 57%. Anal. Calcd for $C_{19}H_{14}Cu_2I_2N_6S_2$: C, 29.58; H, 1.83; N, 10.89. Found: C, 29.55; H, 1.89; N, 10.65%. IR(KBr) ν_{max}/cm^{-1}: 3061m, 1558s, 1538s, 1406m, 1330s, 1185m, 793m, 759m, 717m.

2.3. *X-ray crystallography*

Diffraction intensities for **1**–**5** were collected at 298(2) K on a Bruker SMART CCD-4 K diffractometer employing graphite-monochromated Mo-Kα radiation ($\lambda = 0.71073$ Å). The data were collected using SMART and reduced by SAINT [15]. The structures were solved by direct methods and refined by full-matrix least squares on F^2_{obs} by using SHELXTL-PC package [16]. All non-hydrogen atoms were refined anisotropically, whereas hydrogen atoms were calculated by geometrical methods and refined as a riding model. The crystallographic data for **1**–**5** are listed in table 1 and selected bond lengths (Å) and angles (°) are summarized in table 2.

3. Results and discussion

Reactions between **2-bppm** and various copper salts (e.g., $Cu(NO_3)_2$, CuCl and CuI) are schematically outlined in scheme 1. Slow reaction of $Cu(NO_3)_2$ with **2-bppm** led to two different coordination complexes that differ markedly in color. On the basis of single-crystal X-ray diffraction, the predominant green one, **1**, shows a discrete dinuclear Cu^{2+} macrocyclic structure whereas the minor red one, **2**, has a similar macrocycle motif but based on Cu^+ (*vide infra*). It surprised us that Cu^{2+} was reduced to Cu^+ under such mild conditions given that most Cu^{2+} reductions reported take place under hydro(solvo)thermal conditions especially when interacting with aromatic N donors [17–19]. Unfortunately, the mechanism for Cu^{2+} reduction remains unknown. Complex **2** has Cu^+ bound by four nitrogen atoms from two **2-bppm** and NO_3^- is not coordinated (*vide infra*), stimulating our interest to examine assembly of **2-bppm** with other CuX salts (X = Cl, I). Indeed, self-assembly of CuCl with **2-bppm** also generated intriguing results. In the metal-rich region, a dinuclear Cu^{2+} macrocycle **3** was obtained, in contrast with an analogous Cu^+-based macrocycle **4** in the ligand-rich region. The formation of **3** is apparently initiated by air oxidation of CuCl and contains $CuCl_4^{2-}$. Complex **4** is isostructural to **2** irrespective of different anions (Cl^- *vs.* NO_3^-). The use of stable CuI in place of CuCl resulted in a 1-D chain with Cu_2I_2 dimeric units as nodes and **2-bppm** as bridges (*vide infra*).

Complexes **1**, **3**, and **4** are slightly soluble in methanol but **5** is insoluble in common solvents. Absorption properties of **1**, **3**, and **4** with **2-bppm** were further measured in methanol solution by UV-Vis spectroscopy (Supplementary material). The **2-bppm** shows a strong π–π^* absorption at 263 nm and a weak n–π^* absorption near 313 nm. The spectra for **1** and **3** are similar in appearance to that for **2-bppm**, but **4** displays some vibrational fine structure in the π–π^* absorption region, and a new absorption in lower intensity at 473 nm. The new absorption for **4** is tentatively assigned to the metal-to-ligand charge transfer transition.

Table 1. Crystallographic data and details of structure refinements for **1–5**.

	1	**2**	**3**	**4**	**5**
Formula	$[(C_{19}H_{14}N_6S_2)Cu(NO_3)(H_2O)]_2(NO_3)_2$	$[(C_{19}H_{14}N_6S_2)Cu]_2(NO_3)_2$	$[(C_{19}H_{14}N_6S_2)CuCl]_2(CuCl_4)(H_2O)(CH_3CN)$	$[(C_{19}H_{14}N_6S_2)Cu]_2Cl_2$	$(C_{19}H_{14}N_6S_2)Cu_2I_2$
Formula weight	1192.18	1032.12	1243.42	979.00	771.40
Temperature (K)	298(2)	298(2)	298(2)	298(2)	298(2)
Crystal system	Monoclinic	Orthorhombic	Monoclinic	Orthorhombic	Monoclinic
Space group	$P2_1/c$	*Fddd*	$P2_1/n$	*Fddd*	$C2/c$
Unit cell dimensions (Å, °)					
a	19.9491(8)	10.321(2)	14.481(6)	10.4641(9)	16.496(2)
b	26.176(1)	26.282(5)	21.803(9)	24.520(2)	8.7707(9)
c	19.5164(8)	30.608(6)	15.168(6)	30.341(3)	15.884(2)
α	90	90	90	90	90
β	114.401(2)	90	94.796(5)	90	101.455(1)
γ	90	90	90	90	90
Volume (Å^3), Z	9280.9(7), 8	8302(3), 8	4772(3), 4	7785(1), 8	2252.2(4), 4
Calculated density (g cm^{-3})	1.707	1.651	1.731	1.671	2.275
$F(000)$	4848	4192	2500	3968	1464
Crystal size (mm^3)	$0.41 \times 0.26 \times 0.18$	$0.33 \times 0.21 \times 0.17$	$0.35 \times 0.26 \times 0.18$	$0.15 \times 0.13 \times 0.12$	$0.18 \times 0.15 \times 0.12$
Reflections collected	71,340	14,608	35,535	13,126	7779
Independent reflection	16,343 [R(int) = (0.060)]	2128 [R(int) = (0.048)]	9550 [R(int) = (0.058)]	1721 [R(int) = (0.042)]	1988 [R(int) = (0.035)]
Goodness-of-fit on F^2	1.07	1.01	1.01	1.05	1.05
Final R indices [$I > 2\sigma(I)$]	$R_1 = 0.0490$, $wR_2 = 0.1355$	$R_1 = 0.0449$, $wR_2 = 0.1214$	$R_1 = 0.0420$, $wR_2 = 0.0982$	$R_1 = 0.0294$, $wR_2 = 0.0765$	$R_1 = 0.0276$, $wR_2 = 0.0639$
R indices (all data)	$R_1 = 0.0863$, $wR_2 = 0.1511$	$R_1 = 0.0776$, $wR_2 = 0.1430$	$R_1 = 0.0750$, $wR_2 = 0.1122$	$R_1 = 0.0416$, $wR_2 = 0.0811$	$R_1 = 0.0365$, $wR_2 = 0.0669$
Largest difference peak and hole (e Å^{-3})	−0.43 and 1.92	−0.41 and 0.62	−0.58 and 0.72	−0.22 and 0.34	−0.43 and 0.80

Table 2. Selected bond lengths (Å) and angles (°).

1							
Cu1–N1	1.965(3)	Cu1–N12	1.989(3)	Cu1–O1	1.997(3)	Cu1–N2	2.123(3)
Cu1–N11	2.288(3)	Cu2–N7	1.972(3)	Cu2–N6	1.979(3)	Cu2–O2	1.995(3)
Cu2–N8	2.111(3)	Cu2–N5	2.279(3	Cu3–N24	1.973(3)	Cu3–N13	1.978(3)
Cu3–O3	1.992(3)	Cu3–N23	2.123(3)	Cu3–N14	2.305(3)	Cu4–N18	1.965(3)
Cu4–N19	1.988(3	Cu4–O4	2.005(3)	Cu4–N17	2.133(3)	Cu4–N20	2.264(3)
N1–Cu1–N12	176.0(2)	N1–Cu1–O1	91.4(1)	N12–Cu1–O1	84.6(1)	N1–Cu1–N2	80.9(1)
O1–Cu1–N2	163.1(1)	N1–Cu1–N11	104.3(1)	S1–C10–S2	114.4(2)	S4–C29–S3	114.5(2)
S5–C48–S6	114.1(2)	S7–C67–S8	114.2(2)				
2							
Cu1–N1	2.002(3)	Cu1–N2	2.070(3)	N1–Cu1–N2	80.7(1)	N1–Cu1–N1A	140.2(2)
N2–Cu1–N2A	107.6(2)	S1–C10–S1B	113.0(4)				
3							
Cu1–N12	1.985(3)	Cu1–N2	2.013(3)	Cu1–N11	2.116(3)	Cu1–N1	2.170(3)
Cu1–Cl1	2.2792(12)	Cu2–N7	1.963(3)	Cu2–N5	2.001(3)	Cu2–N6	2.101(3)
Cu2–N8	2.196(3)	Cu2–Cl2	2.308(1)	Cu3–Cl4	2.227(2)	Cu3–Cl3	2.251(2)
Cu3–Cl5	2.254(1)	Cu3–Cl6	2.265(1)	N11–Cu1–N1	100.1(1)	N2–Cu1–N1	78.7(1)
N12–Cu1–N1	113.9(1)	N1–Cu1–Cl1	99.59(9)	N7–Cu2–N5	178.1(1)	N5–Cu2–N6	79.9(1)
N5–Cu2–N8	99.5(1)	N5–Cu2–Cl2	92.68(9)	Cl4–Cu3–Cl3	135.88(6)	Cl3–Cu3–Cl5	100.57(6)
Cl4–Cu3–Cl5	98.23(5)	S3–C10–S1	115.7(2)	S2–C29–S4	115.5(2)		
4							
Cu1–N1	2.010(2)	Cu1–N2	2.082(2)	N1–Cu1–N2	80.47(8)	N1–Cu1–N1A	142.4(1)
N2–Cu1–N2A	105.9(1)	S1–C10–S1B	114.0(2)				
5							
Cu1–I1	2.6323(7)	Cu1–N1	2.087(4)	Cu1–N2	2.094(3)	Cu1–Cu1A	2.539(1)
N1–Cu1–N2	78.9(1)	N1–Cu1–I1	108.7(1)	N2–Cu1–I1	123.90(9)	S1–C10–S1B	114.2(4)

Symmetry codes for **2**: (A) $-x+1/4, -y+1/4, z$; (B) $x, -y+1/4, -z+1/4$; for **4**: (A) $-x+7/4, -y+3/4, z$; (B) $x, -y+3/4, -z-¼$; for **5**: (A) $-x, -y, -z$; (B) $-x, y, -z+1/2$.

3.1. *Structure descriptions for 1–5*

All complexes have been structurally elucidated by X-ray crystallography; **1**–**4** adopt a dinuclear macrocyclic structure whereas **5** shows a 1-D chain structure. The macrocyclic dinuclear metal cations are essentially chiral. The detailed structure descriptions for **1**–**5** follow.

Complex **1** crystallizes in monoclinic crystal system and $P2_1/c$ space group. Each asymmetric unit of **1** consists of two dinuclear macrocyclic structures formulated as [(**2-bppm**)Cu(NO_3)(H_2O)]$_2$ (**1a** and **1b**) related by local non-crystallographic C2 symmetry and four non-coordinated NO_3^- (figure 1). Both **1a** and **1b** are chiral with two stereochemical centers located at two Cu centers, but exist in enantiomeric form due to the centrosymmetric nature of **1**. Except for the stereochemistry around Cu, the structural parameters of **1a** parallel those of **1b**. Taking **1a** as an example, two individual **2-bppm** ligands in **1a** place two Cu^{2+} ions 7.68 Å apart in a bis(chelating) coordination, and the double bipyridine-like arms of each **2-bppm** ligand are arranged above and below the plane defined by –S–CH_2–S–, i.e. in *transoid* configuration. Both $C_{(CH2)}$–S and $C_{(pyrimidine)}$–S bond lengths in **2-bppm** are comparable to the average value for a single C–S bond (1.82 Å) rather than that of double C=S bond (1.62 Å), but the S–S distance are slightly different (3.01 Å *vs.* 3.04 Å). Each Cu^{2+} is in an octahedral coordination, completed by four nitrogen atoms from two ligands, one water molecule,

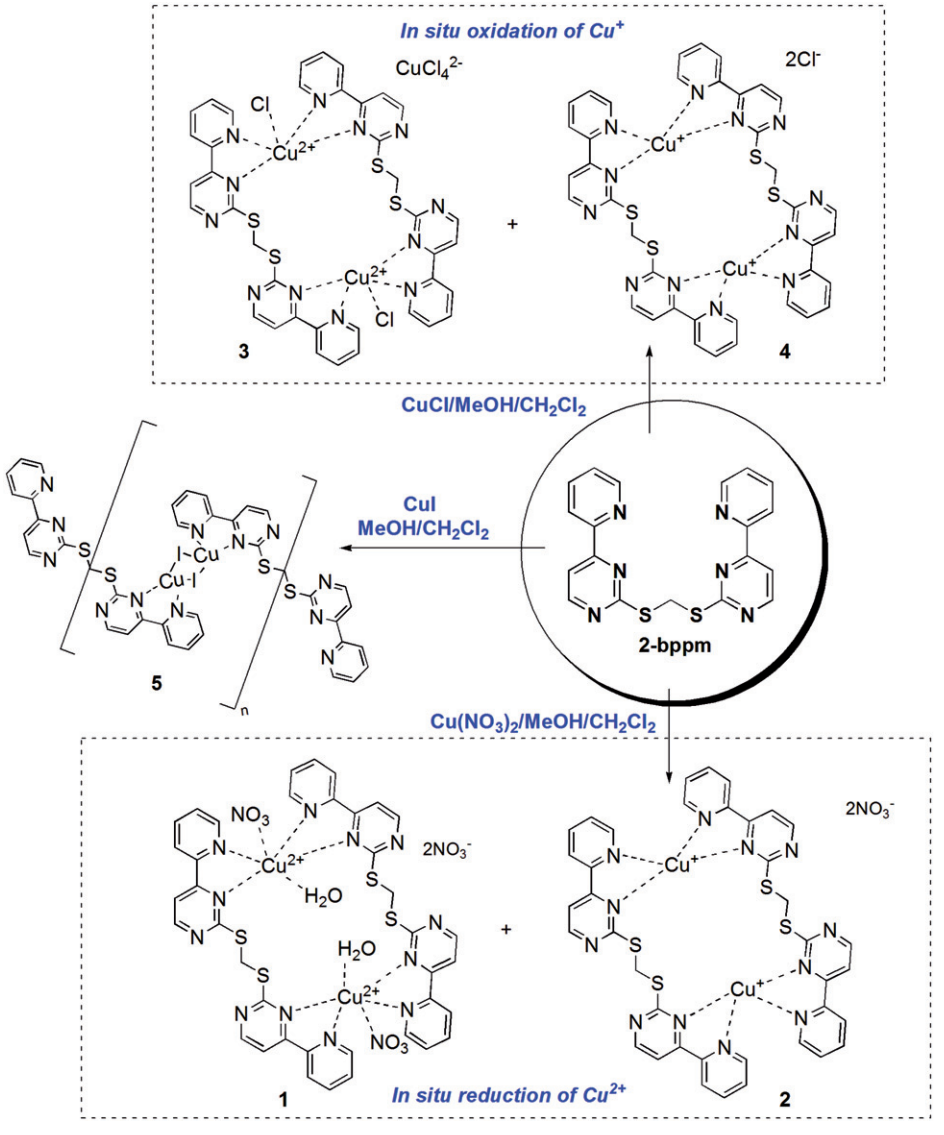

Scheme 1. Variable reactions between **2-bppm** and copper salts.

and one oxygen atom of NO_3^-. Due to Jahn–Teller distortion, both axial Cu–N and Cu–O bond lengths are longer than their counterparts in equatorial positions (see table 2).

Complex **2** crystallizes in orthorhombic crystal system and *Fddd* space group. Although **2** also contains a dinuclear [2 + 2] macrocycle motif, it is exclusively based on Cu^+ due to the occurrence of *in situ* Cu^{2+} reduction (figure 2). The crystal structure of **2** has crystallographic D2 symmetry with two Cu's sitting on a C_2-axis. Similarly, two **2-bppm** in **2** also adopt the *transoid* configuration as found in **1**, separating two isolated Cu^+ ions by 7.72 Å. Compared with **1**, the S···S separation in the –S–CH_2–S– spacer almost remains constant (3.04 Å) but the methylene carbon is disordered over two sites

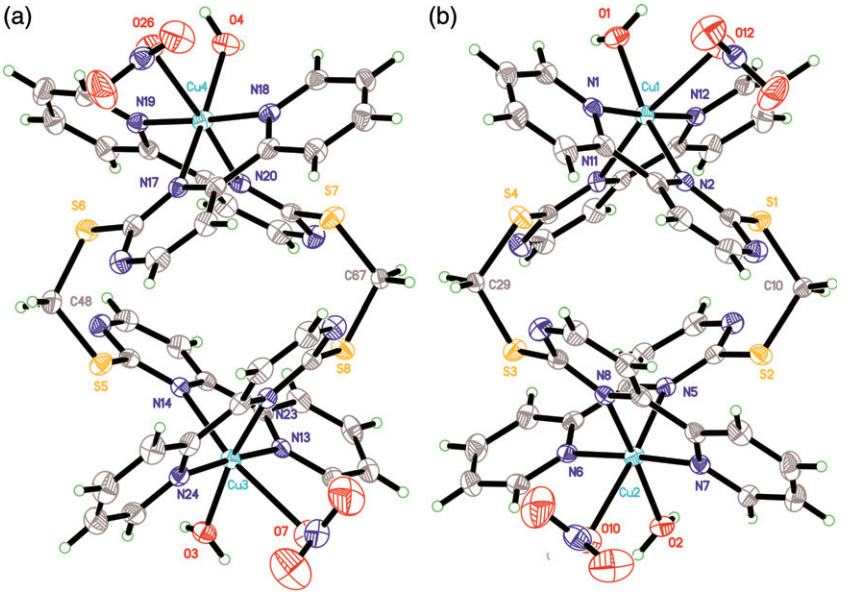

Figure 1. ORTEP view of molecular structure of **1**. Only coordinating atoms with methylene carbon have been numbered and uncoordinated nitrates are omitted for clarity.

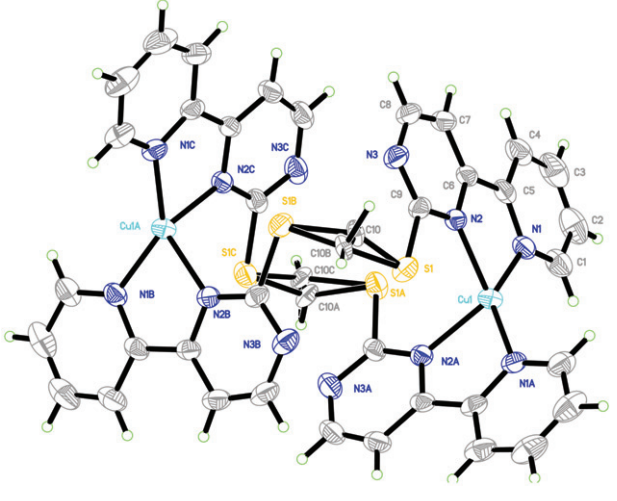

Figure 2. ORTEP view of molecular structure of **2** with the numbering-scheme of selected atoms, and non-coordinated nitrates omitted for clarity.

with half occupancy. It should be noted that each Cu^{+} in **2** is tetrahedral solely by *NN*-donors from two **2-bppm** ligands, and the NO_3^- are not coordinated.

Complex **3** crystallizes in monoclinic crystal system and $P2_1/n$ space group, of which each asymmetric unit is composed of one dinuclear macrocyclic structure $[(\mathbf{2\text{-}bppm})_2Cu_2Cl_2]^{2+}$, one $CuCl_4^{2-}$, one water molecule, and one acetonitrile (figure 3).

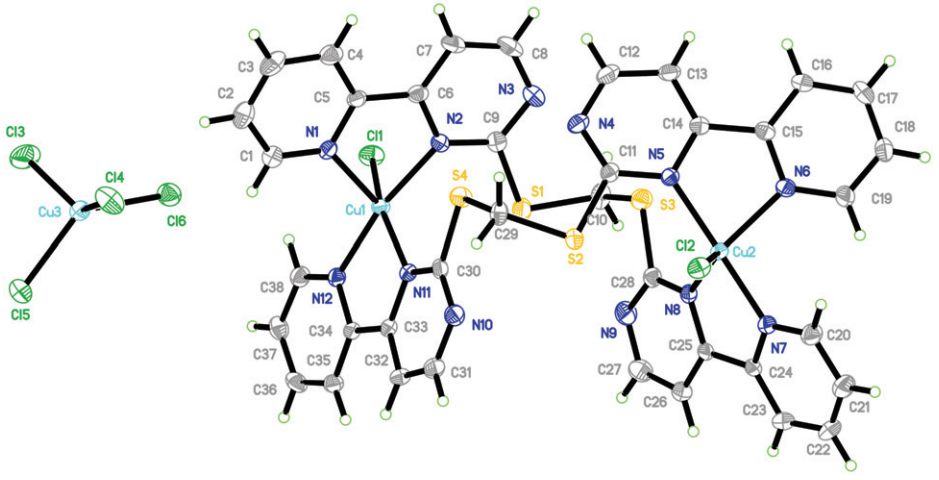

Figure 3. ORTEP view of molecular structure of **3**, and non-coordinated water and acetonitrile are omitted for clarity.

Compared with **1**, the macrocyclic structure of **3**, also constructed by two Cu^{2+} ions doubly bridged by two **2-bppm**, has a larger Cu–Cu distance of 8.56 Å. There exist two independent five-coordinate Cu^{2+} ions, one adopts square-pyramidal geometry with the axial position occupied by one Cl^- and the other is a distorted trigonal-bipyramidal geometry with two nitrogen atoms and a Cl^- in the basal plane and two nitrogen atoms in apical positions. Complex **3** possesses $CuCl_4^{2-}$ that exists as a distorted tetrahedron with Cu–Cl bond lengths varying from 2.227(2) Å to 2.308(1) Å and Cl–Cu–Cl angles from 96.69(6)° to 135.88(6)°.

Complex **4** crystallizes in orthorhombic crystal system and *Fddd* space group, and is isostructural to **2** (figure 4). As a consequence, the crystal structure of **4** also possesses the D2 symmetry wherein two Cu^+ ions are situated on a two-fold axis. Similarly, chloride remains uncoordinated irrespective of its stronger coordinating ability compared to NO_3^-. The strong *NN*-chelating of **2-bppm** coupled with tetrahedral preference of Cu^+ left chloride out of the coordination sphere.

Entirely different from **1**–**4**, **5** has a 1-D chain structure built by alternate linkage of **2-bppm** and Cu_2I_2 dimeric units (figure 5). The **2-bppm** also exhibits a *transoid* configuration that bridges two Cu(I)'s at 7.88 Å. The Cu–Cu separation is 2.54 Å in the dimeric Cu_2I_2 unit that is bonded by chelating *NN*-donors belonging to two **2-bppm**. The reason **5** takes the chain motif instead of the macrocycle structure is likely because **2-bppm** is not suitable for encompassing two Cu_2I_2 units into one macrocycle.

3.2. *Structural comparison and luminescence properties*

By comparing the structural parameters of –S–CH_2–S– spacer in **1**–**5**, –S–CH_2–S– acts as a rigid platform in terms of the S–S distance and SCS angle. The S–S distance is almost constant (*ca* 3.0 Å) and the SCS angle only exhibits minor variations (for **1**, **4** and **5**, avg. 114.2°; for **2**, 112.4°; for **3**, avg. 115.6°). However, the coordinating arms attached to the –S–CH_2–S– platform through $C_{(aromatic)}$–S bonds are quite flexible as

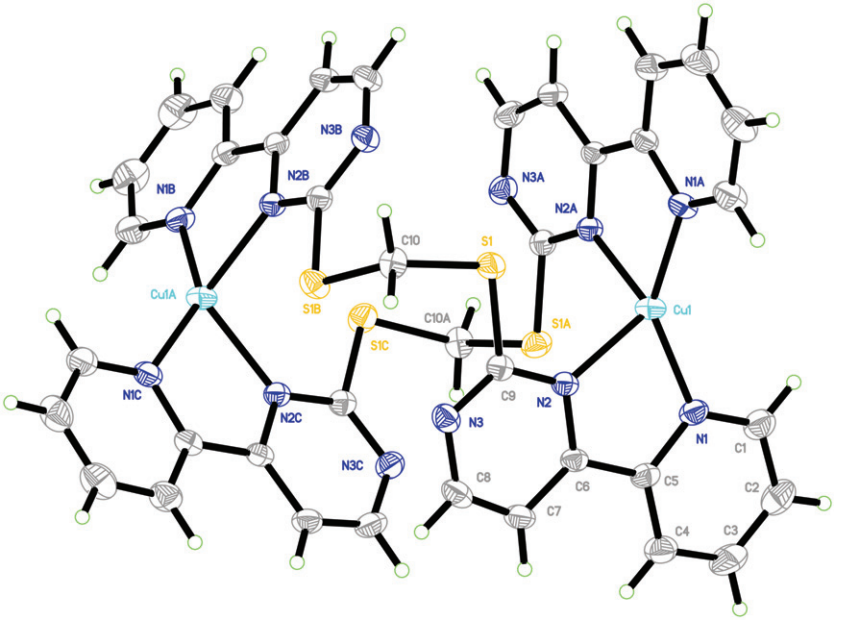

Figure 4. ORTEP view of molecular structure of **4**, and non-coordinated chlorides are not shown for clarity.

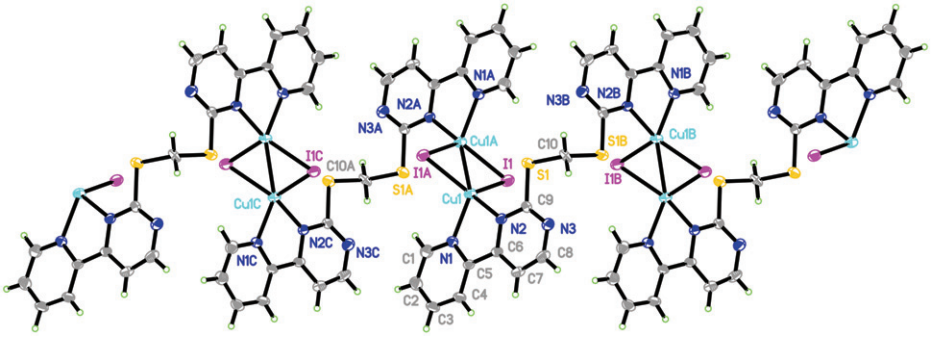

Figure 5. 1-D chain structure of **5**.

indicated by the variable dihedral angles between two pyrimidinyl rings in one **2-bppm**, which span a range from 64.2° to 88.5°. The spatial flexibility of two coordinating arms assures accommodating two Cu's with various coordination geometries into the same macrocycle motif. The *transoid* configuration is preferred by **2-bppm** in all complexes probably due to unfavorable steric encumbrance between the two arms. Compared with the rich coordination chemistry of bis(2-pyridylthio)methane [20], coordination about **2-bppm** seems simple, exclusively based on chelating *NN*-donors. The absence of SN-mixed coordination even in the presence of Cu^{+} might arise from the powerful coordinating ability of *NN*-chelating mode of **2-bppm**.

Generally, of particular interest are d^{10}-closed shell metal coordination complexes owing to their photoluminescence with potential applications in organic light-emitting

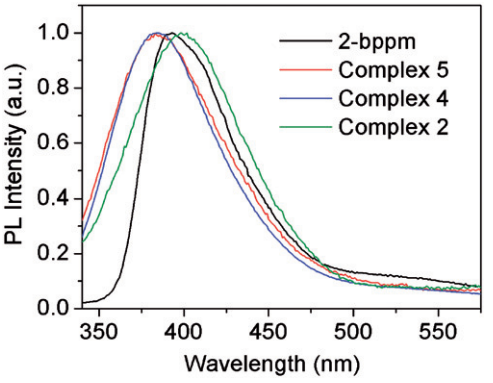

Figure 6. Emission spectra for **2**, **4**, and **5** ($\lambda_{ex} = 320$ nm).

devices, optoelectronic devices, and analytical probes [21]. Accordingly, we investigated the luminescence of **2**, **4**, and **5** that are Cu(I)-based coordination complexes. As depicted in figure 6, the maximum emission peaks of **2**, **4**, and **5** are comparable to that of free **2-bppm**, at *ca* 390 nm upon excitation at 320 nm. Obviously, the photoluminescence properties of the complexes are governed by the **2-bppm**-ligand-centered transition, in accord with observations for Ag(I)/**2-bppm** coordination complexes [12]. Neither the nature of counter-ion (**2** *vs*. **4**) nor the structure motif (**2/4** *vs*. **5**) has obvious impact on the luminescence.

4. Conclusion

This study shows that the redox chemistry of copper ion (Cu^{2+} or Cu^{+}) combined with the flexibility of the organic building blocks would bring about interesting structural variations, which are partly derived from varied coordination geometries of Cu^{2+}/Cu^{+} (e.g., tetrahedron, octahedron, square-pyramid, etc.). On the other hand, it also indicates that the assembled structure is profoundly affected by the nature of counter-ions (**4** *vs*. **5**).

Supplementary material

CCDC 853006–853010 contains the supplementary crystallographic data for this article. These data can be obtained free of charge from The Cambridge Crystallographic Data Centre *via* www.ccdc.cam.ac.uk/data_request/cif

Acknowledgments

We sincerely acknowledge the National Natural Science Foundation of China (Nos 20801011 and 21171036) and Teaching and Research Program for the Excellent Young Teachers of Southeast University (No. 3207042203) for the financial support.

References

[1] B. Moulton, M.J. Zaworotko. *Chem. Rev.*, **101**, 1629 (2001).
[2] J.C. Bünzli, C. Piguet. *Chem. Rev.*, **102**, 1897 (2002).
[3] K. Fromm. *Coord. Chem. Rev.*, **252**, 856 (2008).
[4] K. Biradha, M. Sarkar, L. Rajput. *Chem. Commun.*, 4169 (2006).
[5] T.F. Liu, J. Lü, R. Cao. *CrystEngComm*, **12**, 660 (2010).
[6] F.C. Pigge. *CrystEngComm*, **13**, 1733 (2011).
[7] H.B. Zhu, H. Wang, F. Kong, S.H. Gou, Y.M. Sun. *J. Mol. Struct.*, **99**, 936 (2009).
[8] H.B. Zhu, X. Lu, S.Y. Zhang, W.N. Yang, S.H. Gou. *Inorg. Chim. Acta*, **376**, 694 (2011).
[9] H.B. Zhu, L. Li, G. Xu, S.H. Gou. *Eur. J. Inorg. Chem.*, 1143 (2010).
[10] H.B. Zhu, L. Li, H. Wang, X. Lu, S.H. Gou. *Inorg. Chem. Commun.*, **13**, 30 (2010).
[11] H.B. Zhu, S.H. Gou. *Coord. Chem. Rev.*, **255**, 318 (2011).
[12] H.B. Zhu, S.Y. Zhang, X. Lu, W.N. Yang. *J. Chem. Res.*, **35**, 144 (2011).
[13] X.H. Bu, Y.B. Xie, J.R. Li, R.H. Zhang. *Inorg. Chem.*, **42**, 7422 (2003).
[14] H.B. Zhu, S.Y. Zhang, X. Lu, W.N. Yang, S.H. Gou, J. Chen. *Z. Anorg. Allg. Chem.*, **637**, 1423 (2011).
[15] Siemens. *SAINT (Version 4),* Software Reference Manual, Siemens Analytical X-ray Systems, Inc., Madison, WI (1996).
[16] Siemens. *SHELXTL, (Version 5)*, Reference Manual Siemens Analytical X-ray Systems, Inc., Madison, WI (1996).
[17] S. Banthia, A. Samanta. *Inorg. Chem.*, **43**, 6890 (2004).
[18] J.K. Cheng, Y.G. Yao, J. Zhang, Z.J. Li, Z.W. Cai, X.Y. Zhang, Z.N. Chen, Y.B. Chen, Y. Kang, Y.Y. Qin, Y.H. Wen. *J. Am. Chem. Soc.*, **126**, 7796 (2004).
[19] C.M. Jin, Z. Zhu, M.X. Yao, X.G. Meng. *CrystEngComm*, **12**, 358 (2010).
[20] A. Amoedo-Portela, R. Carballo, J.S. Casas, E. García-Martínez, C. Gómez-Alonso, A. Sánchez-González, J. Sordo, E.M. Vázquez-López. *Z. Anorg. Allg. Chem.*, **628**, 939 (2002).
[21] R.C. Evans, P. Douglas, C.J. Winscom. *Coord. Chem. Rev.*, **250**, 2093 (2006).